Smad3 deficiency alters key structural elements of the extracellular matrix and mechanotransduction of wound closure

Praveen R. Arany*†, Kathleen C. Flanders*†, Tetsu Kobayashi‡, Catherine K. Kuo§, Christina Stuelten*, Kartiki V. Desai*¶, Rocky Tuan§, Stephen I. Rennard‡, and Anita B. Roberts*

*Laboratory of Cell Regulation and Carcinogenesis, National Cancer Institute, National Institutes of Health, Bethesda, MD 20892; ‡Department of Internal Medicine, Pulmonary and Critical Care Medicine Section, University of Nebraska Medical Center, Omaha, NE 68198-5885; and §Cartilage Biology and Orthopedics Branch, National Institute of Arthritis and Musculoskeletal and Skin Diseases, National Institutes of Health, Bethesda, MD 20892

Edited by Joan Massagué, Memorial Sloan–Kettering Cancer Center, New York, NY, and approved April 28, 2006 (received for review March 27, 2006)

The loss of TGFβ or its downstream mediator, Smad3, key players in tissue repair, accelerates closure of incisional wounds in mice. In contrast, we now report that excisional ear wounds in mice lacking Smad3 enlarge compared with wild-type controls resulting from changes in extracellular matrix molecules, which alter the mechanotransduction properties of these wounds. Specifically, levels of elastin and glycosoaminoglycans are increased, collagen fibers are more compactly organized, and matrix modulators like integrins, TGFβ1, and matrix metalloproteinases (MMPs) are altered both basally and after wounding in Smad3 knockout mice. Mechanical testing of dorsal skin correlates these changes in matrix composition with functional parameters, specifically an increased elastic modulus, suggesting an imbalance of tissue forces. We propose that the altered mechanical elastic properties translate into a persistent retractile force that is opposed by decreased wound contractile forces contributing to the enlarging ear wound in Smad3 knockout mice. These studies highlight a previously undescribed role for Smad3 in the mechanotransduction of matrix unsupported ear wound closure.

TGFβ | tissue forces | wound healing

Repair of tissue injury, which involves carefully orchestrated temporal responses and depends on tissue architecture, is the keystone of the organism's ability to maintain physiological homeostasis. Moreover, processes involved in wound healing, including activation of fibroblasts and inflammatory cells and reorganization and synthesis of extracellular matrix (ECM), are paradigmatic for cellular responses in various pathologies, especially fibrosis and cancer. TGFβ, possibly more than any other cytokine, regulates accumulation of ECM proteins as well as their interactions with cells and their actin cytoskeletal structure by means of integrin receptors (1). It can directly stimulate synthesis of proteins such as the collagens and fibronectin, as well as regulate their stability based on altering the balance between matrix-degrading matrix metalloproteinases (MMPs) and tissue inhibitors of MMPs.

Contrary to expectations, improved healing of incisional wounds is observed in mice lacking either TGFβ1 (2) or Smad3 (3, 4), a key cytoplasmic signaling intermediate downstream of the TGFβ receptors. This finding has been based primarily on more rapid closure of these wounds due to effects of loss of TGFβ/Smad3 signaling on keratinocyte proliferation and migration, whereas other aspects of wound healing, including granulation tissue formation and inflammation, are reduced in these models (2–4).

An inbred strain of mice, MRL/MpJ, exhibits a rare amphibious-like trait termed "epimorphic regeneration," characterized by complete functional and structural reconstitution of the injured skin and cartilage in an excisional ear punch wound (5). An aberrant MMP–tissue inhibitors of MMP profile (6) and increased TGFβ1 signaling (7) have both been implicated in this regenerative process. Based on these findings, we investigated the effects of loss of Smad3 in this wound model.

Results

Matrix Unsupported Excisional Ear Wounds Enlarge in Smad3 Knockout (S3KO) Mice. Full-thickness excisional dorsal skin wounds in S3KO mice through to the panniculus carnosa and supported by the underlying matrix show more rapid epithelial closure and reduced wound area compared with their wild-type littermates [Smad3 wild-type (S3WT)] (Fig. 1*A a* and *d*) similar to enhanced healing of incisional dorsal skin wounds in these mice reported previously by us (3). In contrast, similar wounds made in the ears of S3KO, which lack underlying matrix support, enlarged over time compared with S3WT (Fig. 1*A b* and *e*). This difference was more apparent in the pure SVEV129 background alone (Fig. 1*A c* and *f*) as compared with the mixed strain (C57B6 × Black Swiss × SVEV129) used for most of our studies that might harbor individual genetic healing traits, indicating that the deficiency of Smad3 has similar effects in different genetic background.

Although the influx of inflammatory cells was significantly reduced in incisional dorsal skin wounds in S3KO (3), no significant differences were observed in monocyte–macrophage and neutrophil influx into the tissues adjacent to the excisional ear wounds (see Fig. 5*a*, which is published as supporting information on the PNAS web site, and data not shown). To confirm this finding, bone marrow transplants were performed between the genotypes (S3WT to S3KO and vice versa), and successful transplantation was confirmed by complete blood count, FACS, and bone marrow cytospins for Smad3 expression (K.C.F. and A.B.R., unpublished data). No differences in the sequelae of wound healing were observed in either the bone marrow-swapped mice or control mice transplanted with homologous marrow (S3WT to S3WT and S3KO to S3KO) (Figs. 1*B* and 5*b*), demonstrating that the inflammatory response does not play a significant role in the enlargement of matrix-unsupported ear wounds in S3KO mice.

Consistent with the enlarging wounds, we observed increased apoptosis of mesenchymal cells in S3KO ears 24 h after wounding, using an ELISA (Fig. 1*Ca*) and a fluorescent TUNEL assay (Fig. 1*Cb*).

Conflict of interest statement: No conflicts declared.

This paper was submitted directly (Track II) to the PNAS office.

Freely available online through the PNAS open access option.

Abbreviations: αSMA, α smooth muscle actin; DF, dermal fibroblast; ECM, extracellular matrix; FAK, focal adhesion kinase; GAG, glycosoaminoglycan; MMP, matrix metalloproteinase; S3KO, Smad3 knockout; S3WT, Smad3 WT.

†To whom correspondence may be addressed at: Laboratory of Cell Regulation and Carcinogenesis, National Cancer Institute, Building 41, Room C629, 41 Library Drive, Bethesda, MD 20892. E-mail: flanderk@mail.nih.gov or aranyp@mail.nih.gov.

¶Present address: Division of Biomedical Sciences, Johns Hopkins in Singapore, The Nanos, Singapore 138669.

www.pnas.org/cgi/doi/10.1073/pnas.0602473103

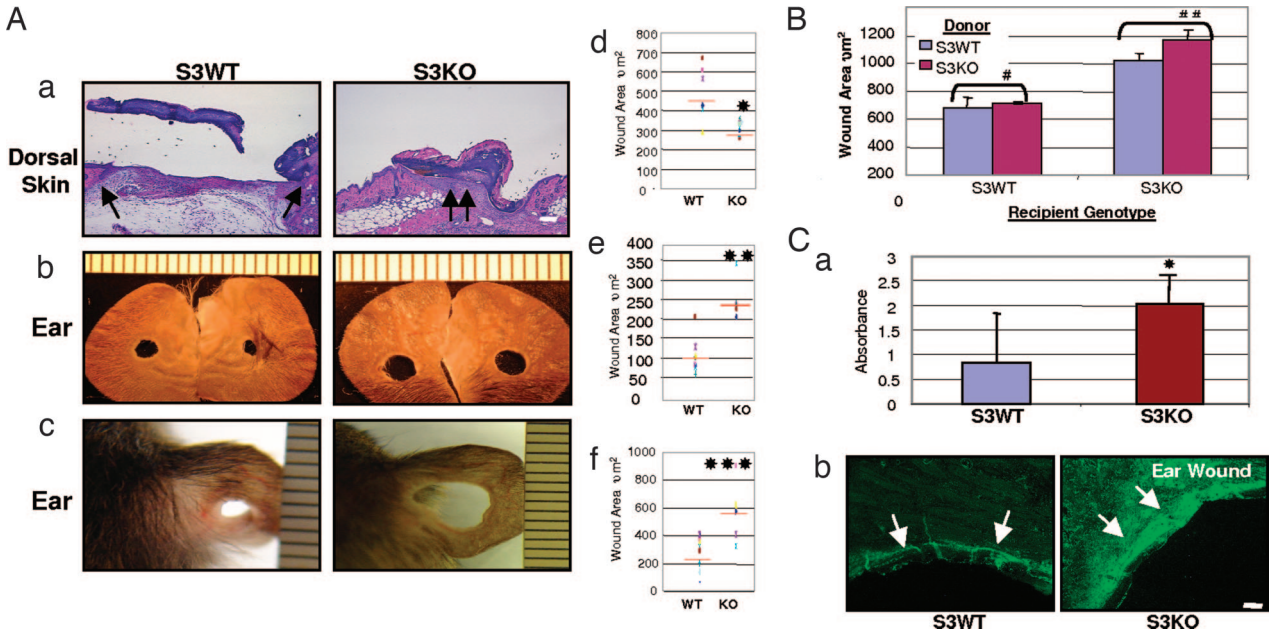

Fig. 1. Excisional would healing in Smad3 mice. (*A*) Smad3-null mice demonstrate opposite wound healing responses in the dorsal skin vs. the ear. (*a*) Dorsal skin 48 h after wounding stained with hematoxylin/eosin. Arrows point to epithelial wound margins. (Scale bar: 100 μm.) (*b*) Ear wounds 38 days after wounding. (*c*) Ear wounds in SVEV129 mice at 36 days after wounding. (*d–f*) Quantification of wound area using a scatter plot. Red bar represents means; $n = 6–8$ mice, *, $P < 0.05$; $n = 3–4$, **, $P < 0.0001$; and ***, $P < 0.05$. (*B*) Quantification of wound area after bone marrow transplantation between genotypes in the healing ear wound at 21 days. $n = 3$ mice. Shown are means ± SD. Healing differences after homologous marrow transplants were not statistically significant: #, $P > 0.5$, and ##, $P > 0.1$. (*C*) (*a*) Quantification of apoptotic cell death in ear wounds by ELISA data represented as means ± SD. $n = 5$; *, $P < 0.05$. (*b*) TUNEL staining of ear wounds at 24 h. Arrows point to a subepithelial prominent band of dermal apoptotic cell at wound edge. (Scale bar: 100 μm.)

Matrix Components Are Altered in S3KO Tissues. Histological staining, immunostaining, ultrastructural analyses, and Western blotting also demonstrated increased elastin protein in S3KO tissues compared with S3WT (Fig. 2*A* and *B*; see also Fig. 6, which is published as supporting information on the PNAS web site). Histochemical staining showed an aberrant organizational arrangement of the elastic fibers and increased elastin fibers anchoring densely packed collagen fibers to the perichondrium in the S3KO ears (Fig. 2*Aa*). We observed both an increased number of elastin fibers in the S3KO tissues and an enhanced electron-dense amorphous core of tropoelastin with disorganized peripheral microfibrils by EM (Fig. 2*Ac*).

Collagen and elastin control the elasticity of the connective tissue, whereas the ground substance consisting predominantly of glycosoaminoglycans (GAGs), stabilizes the fibrillar network and contributes to the stretching and folding pattern of these fibers (8).

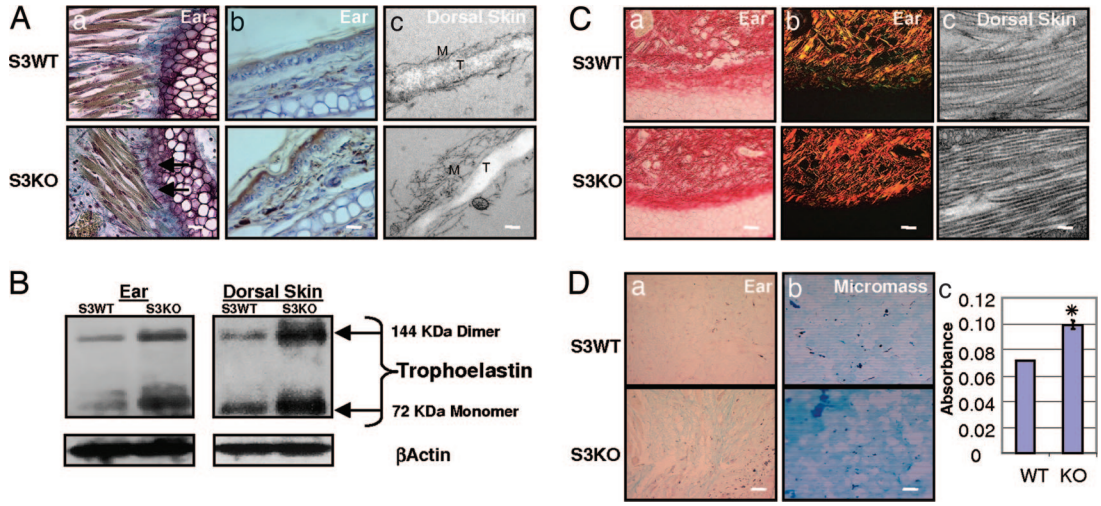

Fig. 2. Matrix components are basally perturbed in S3KO mice. (*A*) Elastin is increased in S3KO tissues as demonstrated by the following. (*a*) Orcein Picroindigocaramine staining. Arrows point to brown coarse elastin fibers tethering collagen fibers to perichondrium in ear. (*b*) Immunohistochemistry in ear. (Scale bars for *a* and *b*: 25 μm.) (*c*) EM of dorsal skin demonstrates increased tropoelastin (T) core and disorganized microfibrillar (M) peripheral sheath of elastin fibers in S3KO dorsal skin. (Scale bar: 0.2 μm.) (*B*) Western blot for elastin. (*C*) Collagen fibers stained by Picrosirius staining and polarizing microscopy. (*a*) Phase contrast. (*b*) Polarizing filters. (Scale bars for *a* and *b*: 50 μm.) (*c*) EM of dorsal skin revealed condensed fibrillar arrangement. (Scale bar: 0.2 μm.) (*D*) (*a*) GAGs visualized by alcian blue (pH 1) staining in ears. (Scale bar: 125 μm.) (*b*) Micromass cultures of primary DFs. (Scale bar: 50 μm.) (*c*) Quantification of GAG expression in these cells by spectrophotometery, showing means ± SD. *, $P < 0.01$.

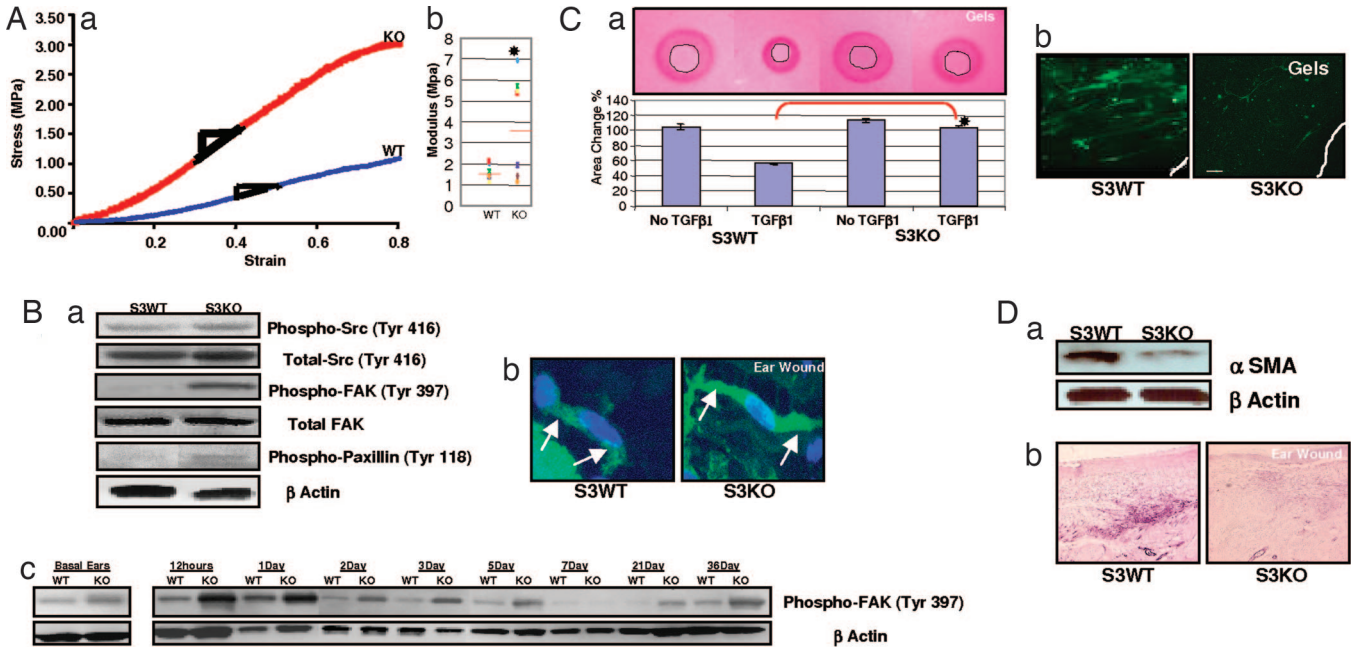

Fig. 3. Tissue mechanical properties and forces are altered in S3KO mice. (*A*) (*a*) Stress vs. strain plots of dorsal skin in linear region in representative sample curves. (*b*) Scatterplot of modulus of individual samples. Red bar represents means; $n = 7$ or 8 samples; *, $P < 0.05$. (*B*) (*a*) Wound tissue analyzed for stress-associated signaling and adhesion molecules at 12 h after wounding. (*b*) Stress fibers at 24 h after wounding in ear tissues demonstrated (arrows) in individual fibroblasts by phalloidin staining and counterstained with DAPI. (Scale bar: 7 μm.) (*c*) Time course analysis of phospho-FAK levels by Western blots. (*C*) (*a*) Primary DFs in annular collagen–elastin gels in the presence or absence of TGFβ1 (2.5 ng/ml) at 5 days (*Upper*) and quantification of contracted central annular gel area (*Lower*). Shown are means ± SD; $n = 3$; *, $P < 0.001$. (*b*) αSMA immunostaining in gels. (Scale bar: 100 μm.) (*D*) Wound tissues at 7 days analyzed for αSMA by Western blotting (*a*) and immunostaining (*b*). (Scale bar: 125 μm.)

Picrosirius red staining and polarizing microscopy showed more densely packed collagen fibers in the ears and dorsal skin of S3KO mice (Fig. 2*C*; see also Fig. 7 *a* and *c*, which is published as supporting information on the PNAS web site). Ultrastructural analyses also demonstrated that individual collagen fibrils had a significantly decreased diameter in ears of S3KO mice (Fig. 7*b*). Both the coarse collagen fibers and increased fibrillar molecules per unit area together suggest there might be increased crosslinking (9). Previous studies have demonstrated no differences in total basal collagen content (hydroxyproline) in S3KO compared with S3WT mice (10), whereas we show here that there are differences in the architectural organization.

The GAGs are covalently linked by polysaccharide chains to core proteins forming proteoglycans. The relative abundance of the polysaccharide chains and their ability to control the level of hydration of tissues, especially of elastin, determines in part the physical properties of connective tissue (11, 12). Elastin has been shown to affect GAG synthesis through the elastin–laminin receptor (13), and GAGs in turn have been shown to affect elastin synthesis and arrangement (14). Histochemical staining demonstrated increased basal GAG levels in S3KO ears *in vivo* (Fig. 2*Da*) and in *in vitro* assay with micromass cultures of primary dermal fibroblasts (DFs) (Fig. 2*D b* and *c*).

Increased Elastic Modulus in S3KO Tissues. Given the similar basal perturbations in ECM components in dorsal skin and ear, we next examined the mechanical properties of intact dorsal skin of these mice to test our hypothesis that the enlarging S3KO ear wounds might result from disproportionate changes in tissue forces. During mechanical testing, resistance to tension by straightening, uncoiling, or unfolding of fibrils and molecules results in the linear region of the stress–strain curve, the modulus of which is often defined as modulus of elasticity. S3KO dorsal skins showed an increase in modulus in both the toe and linear region as compared with S3WT (Fig. 3*A*; see also Fig. 8, which is published as supporting information on the PNAS web site). A higher modulus of elasticity can be due to effects such as increased fibrillar molecules per unit area, increased fibril diameter, or increased crosslinking of fibrillar molecules. These changes are consistent with our observation of the perturbed matrix composition in S3KO mice.

Postwounding Tissue Mechanical Responses Are Perturbed in S3KOs. Based on these basal ECM perturbations and altered mechanical properties of the S3KO matrix, we predicted an exaggerated tissue force in the ear after wounding, possibly contributing to the enlarging wound phenotype. We observed an increased expression of molecular markers of focal adhesion signaling in S3KO ears at 12 and 24 h after wounding including phospho-Src (at Tyr-416 but not Tyr-527), which up-regulates its enzyme activity (15); phospho-focal adhesion kinase (FAK) (Tyr-397), which is induced by extracellular integrin clustering (16); and phospho-paxillin (Tyr-118), which is phosphorylated by FAK (17), ultimately increasing local assembly of F-actin resulting in the morphological "stress fiber" phenotype (Fig. 3*B a* and *b*). The increased basal phospho-FAK in S3KO might indicate increased cellular prestress as a result of the perturbed matrix, whereas time course analyses of wounds demonstrated a phasic pattern, i.e., early increase for 12–24 h, decreased at 5–7 days and then remained elevated at late time points in S3KO wounds (Fig. 3*Bc*).

Myofibroblast-Mediated Contraction Is Decreased in S3KOs. Fibroblasts can generate tractional forces and are thought to ensure tissue tensional homeostasis (18). Smad signaling has been shown to be critical for TGFβ-dependent contraction of collagen gels by fibroblasts (19). We now show that S3KO DFs cells do not contract a central annular hole, simulating the excisional ear wound, in collagen–elastin gels suggesting that contractile forces might be severely reduced in the S3KO ear wounds (Fig. 3*Ca*; see also Fig.

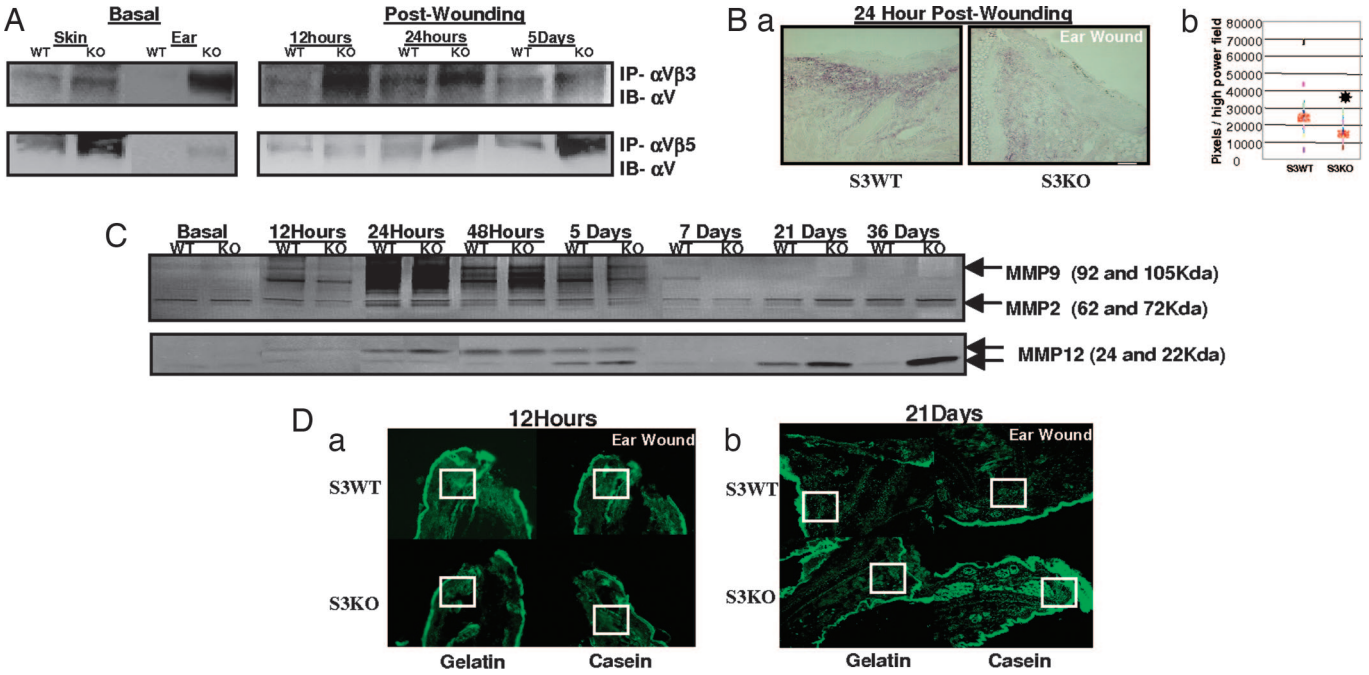

Fig. 4. Matrix modulators are perturbed in S3KO. (*A*) Immunoprecipitations with tissue extracts performed with specific integrin complex antibodies, $\alpha V\beta 3$ and $\alpha V\beta 5$, and immunoblotted with αV antibody. (*B*) Wound margins analyzed for TGFβ1 at 24 h by immunostaining (*a*) and quantification (*b*). Red bar represents means; $n = 5$; *, $P < 0.05$. (Scale bar: 125 μm.) (*C*) Time course substrate-specific zymography for MMP2 and MMP9 (gelatin; *Upper*) or MMP12 (casein; *Lower*). (*D*) *In situ* zymography on cryosections using fluorescent substrate overlays 12 h (*a*) and 21 days (*b*) after wounding. (Scale bars: 200 μm.) Boxed areas show prominent enzymatic activity.

9 *b* and *c*, which is published as supporting information on the PNAS web site). TGFβ1 can induce α smooth muscle actin (αSMA), considered a hallmark of myofibroblasts and associated with the contractile phenotype *in vivo* (20) and contraction in collagen gels *in vitro* (21), in S3KO DFs in monolayer cultures (see Fig. 10 *a* and *b*, which is published as supporting information on the PNAS web site) (22), but not in free floating collagen-elastin gels (Fig. 3C*b*), suggesting that there is an uncoupling of S3KO responses as has been reported (23, 24). Moreover, S3KO DFs in these gels did not assemble F-actin (Fig. 9*a*) and appeared rounded and randomly distributed along the gel edges, whereas S3WT DFs were stellate shaped and arranged parallel to the gel edge typical of the "contractile phenotype" (25). We also observed a decreased αSMA expression in S3KO ears 7 days after wounding *in vivo* (Fig. 3*D a* and *b*) suggestive of decreased wound contraction.

Matrix Modulators in S3KO Mice Are Perturbed After Wounding. Changes in integrin expression have been implicated in wound healing both in migration of epithelial cells (26) and in contraction by myofibroblasts (27). We demonstrate increased expression of elastin-binding integrins $\alpha V\beta 3$ and $\alpha V\beta 5$ (28) basally in S3KO ears. Although $\alpha V\beta 3$ increased significantly 12 and 24 h after wounding and decreased at 5 days compared with S3WT, gradual increase in $\alpha V\beta 5$ expression was seen up to 5 days after wounding (Fig. 4*A*).

Many enzymes and cytokines regulate ECM expression at the transcriptional and posttranscriptional level, and TGFβ1 figures prominently among them (1). Quantification of TGFβ1 immunostaining showed decreased TGFβ1 expression 24 h after wounding in S3KO ears (Fig. 4*B*) in contrast to the reported increase seen in TGFβ1 levels in regenerating ear wounds in MRL mice (7).

The major matrix modulators responsible for remodeling and maintaining connective tissue homeostasis are the MMPs (29). MRL mice exhibit increased MMP2 and -9 activity early after wounding suggesting its role in mediating regeneration (6). In contrast, wounds in S3KO ears showed an initial decrease in MMP9 activity as compared with S3WTs at 12 h persisting to up to 7 days, whereas later time points (21 and 36 days) showed increased activity (Fig. 4*C*). MMP2 activity was unaltered.

It was reported that the S3KO macrophages play a key role in mediating age-dependent lung emphysema in S3KO mice by upregulating MMP12 mRNA (30). Although macrophage infiltration was unchanged in our wound model, MMP12 activity decreased at 12 h after wounding but increased at late time points, similar to MMP9 (Fig. 4*C*). The absence of a significant inflammatory component in our healing model was evident from the bone marrow swapping experiments (Figs. 1*B* and 5), emphasizing that inherent immune cell functionality also requires appropriate external microenvironment cues. *In situ* zymography demonstrated these phasic changes in MMPs to be specifically localized to the matrix (Fig. 4*D*).

Discussion

We have described a unique biological model where a single missing gene, Smad3, has dramatically opposite effects on wound healing in the presence or absence of underlying tissue support, providing previously undescribed insights into the different roles of constituent cells and matrix in these two contexts. Loss of Smad3 results in a more rapid closure of excisional wounds with underlying matrix support on the mouse dorsum, whereas a similar wound made on the ear, with no matrix support, shows an exacerbated enlarging wound phenotype.

Wound healing is affected both by tissue architecture and the participating cell types and, as highlighted in this work, the presence or absence of underlying tissue support. Healing of wounds on the skin is affected primarily by changes in epithelial migration and inflammatory influx, whereas these processes had a redundant role in the matrix-unsupported ear wounds, possibly due to the absence of a rich vascular network and apparent lack of a granulation tissue in the ear. Studies are needed to analyze contributions of these anatomical differences, including the vasculature and cartilage core,

both of which are affected by loss of Smad3 (31, 32). It is important to note that there is no wound breakdown, i.e., epithelial ulceration or cartilage extroversion, throughout the healing phases, suggesting that both these components are remodeled to maintain tissue homeostasis. Although basal matrix compositions are similar in S3KO ear and dorsal skin, wound architecture and changes after wounding in MMPs, stress-activated signaling, and GAG staining patterns distinguish the two (P.R.A. and A.B.R., unpublished data). Studies both in mice (3, 4) and in the rabbit ear (33) support opposite effects of Smad3 on keratinocyte (accelerated migration) and on mesenchymal (reduced granulation tissue) wound healing. In the absence of a matrix, as in the excisional ear wound, effects of the loss of Smad3 in the mesenchyme might predominate in the ultimate wound outcome.

It is now accepted that structure and function in tissues are intimately related and that alterations in tissue structure, including the ECM, can result in perturbed biological responses (34). Tissue microforces have been widely studied in various contexts, including mineralizing bone, vascular physiology, tissue–organ morphogenesis, and differentiating immune cells, and also have been therapeutically exploited to remodel tissues and organs such as vessels, bone, and soft tissues or change tooth alignment. Perturbed tissue forces can lead to pathological conditions as in contractures, degenerative joint disorders, and cardiac dysfunction (35, 36). The major limitation of our present study is the inability to measure actual tissue forces before and after wounding *in vivo* and reliably perform similar mechanical testing of ear (cartilage core and limited physical dimensions) as with the dorsal skin. We thus can only speculate that the similarities of basal Smad3-dependent alterations in matrix constituents in the dorsal skin (epithelium and matrix) and ears (epithelium and matrix but not cartilage) would predict similar tissue mechanical behavior after wounding. The increased elastic modulus in S3KO tissues, also reported in their bones (37), may translate into an enhanced retractive force in S3KO ears after wounding (see Fig. 11, which is published as supporting information on the PNAS web site). Our data showing altered expression of integrin receptors, also called cell surface "mechanoreceptors" (38), increased stress fibers, and prolonged activation of focal adhesion-mediated signaling, which could be considered "surrogate markers," demonstrate these altered tissue forces in S3KO wounds. We are presently exploring differences between S3WT and S3KO in their crosslinking status of elastin and collagen as well as individual types of collagen fiber and GAG components that are key facets of the matrix organization and function.

Decreased TGFβ1 after wounding (Fig. 4*B*) and altered ECM mechanical properties might both contribute to an *in vivo* uncoupling phenomenon in the S3KO ear wounds that have been shown to be critical in determining the myofibroblastic phenotype (23, 24). In lieu of the phasic nature of wound contraction (Fig. 10*c*) and its inability to counteract gaping wound forces continuously, we believe the decreased αSMA alone is not sufficient to explain the progressively enlarging ear wound in S3KOs. Our analyses demonstrated that in the absence of an effectual inflammatory component, the major cellular source of MMPs, there was still a significant matrix remodeling phase in S3KO ear wounds as reflected by the increased MMP9 and -12 activity late after wounding (Fig. 4 *C* and *D*), which correlates with the timing of the observed enlarging ear wounds. Altered tissue forces in the S3KO matrix might play a key role in initiating these MMPs as has been shown (39). Also, matrix degradation products, especially of elastin, can act as "matrikines" (12) all together resulting in aggravated matrix remodeling and contributing causally to the enlarging S3KO wound phenotype.

Our observation of increased elastin in the absence of Smad3 raises the possibility that alterations in Smad3 expression or function might contribute to "elastinopathies," broadly defined as genetic or functional aberrancies in elastin structure–function, such as supravalvular aortic stenosis, cutis laxa, solar elastosis, and atherosclerosis (40). Moreover, the role of elastin in tumorigenesis is a little researched area (41), and our model may provide a previously undescribed framework to analyze its contributions in terms of physiochemical and molecular interactions. Tumors have been described as wounds that do not heal (42), as well as overhealing wounds (43), and a strong correlation between an activated wound gene expression profile and metastasis has been shown (44). Further, a study done on the anatomical site susceptibility of tumor metastasis in mice demonstrated decreased metastatic spread from the ear compared with the tail or dorsum (45). Our demonstration of accelerated healing in S3KO mice on the dorsum and tails (3, 4), yet poorer healing in the ear, suggests that unlike conventional "passive" transgenic animal models used to study tumor–stromal microenvironment, the use of an "active" wound matrix might aid a finer dissection of the dynamic interactive factors in promoting tumor growth and metastasis. Tissue forces as a physical determinant of tumors are being studied in the context of mechanophysical properties of individual tumor cell and tumor–stroma in predicting tumor behavior (46–48). We speculate that our demonstration of similar changes in matrix composition and increased tensional forces, especially the associated prolonged activation of phospho-FAK (Tyr-397) in the Smad3-null mouse might be extended to address similar questions in cancer biology.

Materials and Methods

Animal Studies. All procedures were approved by the institutional animal care and use committee. Dorsal skin of 4- to 6-week-old mice in mixed strain of C57B6/Black Swiss/SVEV129 or SVEV129 (only wounding experiment) mice was shaved, and wound sites were swabbed with alcohol and povidone. Excisional 4-mm punches (Acuderm, Fort Lauderdale, FL) were made on the central aspect of the pinna or dorsal skin. Wounds and basal (unwounded) tissues were harvested at given time points.

Bone Marrow Transplants. Donor mice (n = 1 or 2) and recipients (n = 3–5) of each genotype were used for bone marrow isolation using the Magnetic Cell Sorting (MACS) system (Miltenyi Biotec, Auburn, CA) according to the manufacturer's instructions. Tail vein injections were performed with 1×10^6 cells per 100 μl per recipient 6 h after lethal irradiation. Mice were allowed to recover for 3 weeks before wounding.

Cell Culture. Primary DFs were isolated from S3WT and S3KO 2-day-old pups. Cells were propagated in 10% FBS (HyClone) DMEM/1% Penstrep (GIBCO) and used between two and seven passages for all assays.

Histological Analysis. Tissues were fixed in 10% buffered formalin and processed for histochemical staining including hematoxylin/eosin or special stains such as orcein–picroindigocaramine for elastin, picrosirius red F3B and polarizing microscopy for collagen, or alcian blue (pH 1.0) and neutral red. Histological analyses were performed with a light microscope (Leica) and digital imaging software (IMAGE-PRO PLUS; Media Cybernetics, Silver Spring, MD).

Immunohistochemistry. Sections were deparaffinized, hydrated, blocked for endogenous peroxidase and secondary antibody animal sera, and incubated with the primary antibody (see Table 1, which is published as supporting information on the PNAS web site) followed by appropriate species specific secondary antibody and diaminobenzidine or very intense purple (Vector Laboratories) according to manufacturer's instructions.

Gels. After 5 days, gels were fixed in 4% paraformaldehyde, permeabilized with 0.5% Triton X-100, and stained for αSMA (Sigma).

Ultrastructural Analyses. Mouse skin and ear were fixed in cacodylate buffer and processed for embedding in epoxy resin, thin sectioned, stained in uranyl acetate and lead citrate for electron microscopy (Model H7000; Hitachi. Tokyo), and images were captured with a digital camera.

Immunoprecipitations and Western Blot. Wound samples were collected in RIPA buffer (150 mM NaCl/10 mM Tris·HCl, pH 7.4/1% Nonidet P-40/1% sodium deoxycholate/0.1% SDS) with Complete Mini Protease inhibitor mixture (Roche), were electrophoresed in precast Tris·glycine gels (Invitrogen), and transferred onto 0.2-μm nitrocellulose membranes (Amersham Pharmacia). Blots were incubated with primary antibodies (Table 1) and appropriate species-specific secondary antibody (The Jackson Laboratory), and chemiluminescence (Pierce) was detected by films or digital imager (Alpha Innotech, San Leandro, CA). Immunoprecipitation was performed with 200 μg per 200 μl of lysate incubated with integrin-specific antibodies (above) at 4°C overnight; specific complexes were pulled down with GammaBind (Amersham Pharmacia), and 4× SDS lysis buffer was added and heated at 95°C for 10 min followed by Western blotting analysis.

Gel and *in Situ* Zymography. RIPA-extracted tissue lysates (10–20 μg) were separated in gelatin and casein precast gels (Invitrogen) at 100 mV, incubated in renaturing buffer for 30 min, and then incubated in developing solution for 18–24 h until proteolytic clear bands were visualized by Coomassie staining. *In situ* zymography was performed on thawed cryosections overlaid with substrate (50 mg/ml DQ gelatin and 200 μg/ml fluorescein-labeled casein; Invitrogen), and degradation products were visualized by fluorescence microscopy.

Mechanical Testing. Dorsal skin was shaved and dissected; snap frozen, and stored at −70°C. Before testing, skins were thawed for 30 min, soaked in PBS, and mounted between grips on an ELectroForce ELF 3200 (EnduraTEC Systems Group, Bose Corp., Eden Prairie, MN). Skins were preloaded to 0.15 N at 0.2% per sec constant strain rate where a digital image was captured, and loading continued until failure. Cross-sectional area was calculated from the product of the histological thickness and width (digital image) and gage length (prior original gage length and displacement at preload). Stress was calculated by normalizing force data to cross-sectional area. Displacement data were converted to strain (change in length/gage length at preload). A stress–strain curve was generated, from which toe-region (range of 2% strain) and linear-region (inflection point) moduli were determined. The ranges of strain, in which toe-region and linear-region moduli were calculated, were chosen as the maximum ranges for greatest accuracy.

Three-Dimensional Collagen Gel Contraction Assays. Collagen–elastin gels prepared by mixing collagen (0.75 mg/ml), α-elastin (0.05 mg/ml), and 5×10^5 cells per ml DFs into each well of a 24-well culture plate, using a yellow pipette tip placed in the center to produce the annular pattern. After 20 min, gels were gently released and transferred into 60-mm tissue culture dishes (three gels per dish), containing 5 ml of 0.1% FCS–DMEM with/without TGFβ1 (2.5 ng/ml) and incubated at 37°C in a 5% CO_2 atmosphere. Gel area was measured with an image analyzer (Optomax, Burlington, MA), and data were expressed as the percentage of area compared with initial gel areas.

Apoptosis Assays: Fluorescent TUNEL and Cell-Death ELISA. Assays (both from Roche) were performed according to manufacturer's instructions on formalin-fixed paraffin-embedded sections and tissue lysates.

Statistical Analyses. EXCEL (Microsoft) was used for statistical analyses and the two-tailed unpaired *t* test to determine significance (*P* values).

Additional details are provided in *Supporting Materials and Methods*, which is published as supporting information on the PNAS web site.

We thank Akira Ooshima, Tatiana S. Karpova, Dalit Barkan, and Kunio Nagashima for imaging facilities; Philip Steven for orcein picroindigocaramine protocol; Anastasia Sowers, Mario Anzano, Anthony Vieira, and Larry Mullen for help with mice; and Benjamin Ho, Zhonghui Sun, and Shawheen Shomolo for help with experiments. This work was supported by the National Institutes of Health Intramural Research Program, National Cancer Institute, Center for Cancer Research.

1. Kim, L. T. & Yamada, K. M. (1997) *Proc. Soc. Exp. Biol. Med.* **214,** 123–131.
2. Koch, R. M., Roche, N. S., Parks, W. T., Ashcroft, G. S., Letterio, J. J. & Roberts, A. B. (2000) *Wound Repair Regen.* **8,** 179–191.
3. Ashcroft, G. S., Yang, X., Glick, A. B., Weinstein, M., Letterio, J. L., Mizel, D. E., Anzano, M., Greenwell-Wild, T., Wahl, S. M., Deng, C., *et al.* (1999) *Nat. Cell Biol.* **1,** 260–266.
4. Falanga, V., Schrayer, D., Cha, J., Butmarc, J., Carson, P., Roberts, A. B. & Kim, S. J. (2004) *Wound Repair Regen.* **12,** 320–326.
5. Clark, L. D., Clark, R. K. & Heber-Katz, E. (1998) *Clin. Immunol. Immunopathol.* **88,** 35–45.
6. Gourevitch, D., Clark, L., Chen, P., Seitz, A., Samulewicz, S. J. & Heber-Katz, E. (2003) *Dev. Dyn.* **226,** 377–387.
7. Kench, J. A., Russell, D. M., Fadok, V. A., Young, S. K., Worthen, G. S., Jones-Carson, J., Henson, J. E., Henson, P. M. & Nemazee, D. (1999) *Clin. Immunol.* **92,** 300–310.
8. Cavalcante, F. S., Ito, S., Brewer, K., Sakai, H., Alencar, A. M., Almeida, M. P., Andrade, J. S., Jr., Majumdar, A., Ingenito, E. P. & Suki, B. (2005) *J. Appl. Physiol.* **98,** 672–679.
9. Wollensak, G., Wilsch, M., Spoerl, E. & Seiler, T. (2004) *Cornea* **23,** 503–507.
10. Lakos, G., Takagawa, S., Chen, S. J., Ferreira, A. M., Han, G., Masuda, K., Wang, X. J., DiPietro, L. A. & Varga, J. (2004) *Am. J. Pathol.* **165,** 203–217.
11. Quinn, T. M., Dierickx, P. & Grodzinsky, A. J. (2001) *J. Biomech.* **34,** 1483–1490.
12. Duca, L., Floquet, N., Alix, A. J., Haye, B. & Debelle, L. (2004) *Crit. Rev. Oncol. Hematol.* **49,** 235–244.
13. Fodil-Bourahla, I., Drubaix, I. & Robert, L. (1999) *Mech. Ageing Dev.* **106,** 241–260.
14. Fornieri, C., Baccarani-Contri, M., Quaglino, D., Jr., & Pasquali-Ronchetti, I. (1987) *J. Cell Biol.* **105,** 1463–1469.
15. Hunter, T. (1987) *Cell* **49,** 1–4.
16. Cobb, B. S., Schaller, M. D., Leu, T. H. & Parsons, J. T. (1994) *Mol. Cell. Biol.* **14,** 147–155.
17. Bellis, S. L., Miller, J. T. & Turner, C. E. (1995) *J. Biol. Chem.* **270,** 17437–17441.
18. Sawhney, R. K. & Howard, J. (2002) *J. Cell Biol.* **157,** 1083–1091.
19. Kopp, J., Preis, E., Said, H., Hafemann, B., Wickert, L., Gressner, A. M., Pallua, N. & Dooley, S. (2005) *J. Biol. Chem.* **280,** 21570–21576.
20. Tomasek, J. J., Gabbiani, G., Hinz, B., Chaponnier, C. & Brown, R. A. (2002) *Nat. Rev. Mol. Cell Biol.* **3,** 349–363.
21. Arora, P. D. & McCulloch, C. A. (1994) *J. Cell Physiol.* **159,** 161–175.
22. Flanders, K. C., Major, C. D., Arabshahi, A., Aburime, E. E., Okada, M. H., Fujii, M., Blalock, T. D., Schultz, G. S., Sowers, A., Anzano, M. A., *et al.* (2003) *Am. J. Pathol.* **163,** 2247–2257.
23. Desmouliere, A., Chaponnier, C. & Gabbiani, G. (2005) *Wound Repair Regen.* **13,** 7–12.
24. Arora, P. D., Narani, N. & McCulloch, C. A. (1999) *Am. J. Pathol.* **154,** 871–882.
25. Costa, K. D., Lee, E. J. & Holmes, J. W. (2003) *Tissue Eng.* **9,** 567–577.
26. Clark, R. A., Ashcroft, G. S., Spencer, M. J., Larjava, H. & Ferguson, M. W. (1996) *Br. J. Dermatol.* **135,** 46–51.
27. Lygoe, K. A., Norman, J. T., Marshall, J. F. & Lewis, M. P. (2004) *Wound Repair Regen.* **12,** 461–470.
28. Nakamura, T., Lozano, P. R., Ikeda, Y., Iwanaga, Y., Hinek, A., Minamisawa, S., Cheng, C. F., Kobuke, K., Dalton, N., Takada, Y., *et al.* (2002) *Nature* **415,** 171–175.
29. Ravanti, L. & Kahari, V. M. (2000) *Int. J. Mol. Med.* **6,** 391–407.
30. Bonniaud, P., Kolb, M., Galt, T., Robertson, J., Robbins, C., Stampfli, M., Lavery, C., Margetts, P. J., Roberts, A. B. & Gauldie, J. (2004) *J. Immunol.* **173,** 2099–2108.
31. Yang, X., Chen, L., Xu, X., Li, C., Huang, C. & Deng, C. X. (2001) *J. Cell Biol.* **153,** 35–46.
32. Kobayashi, K., Yokote, K., Fujimoto, M., Yamashita, K., Sakamoto, A., Kitahara, M., Kawamura, H., Maezawa, Y., Asaumi, S., Tokuhisa, T., *et al.* (2005) *Circ. Res.* **96,** 904–912.
33. Sumiyoshi, K., Nakao, A., Setoguchi, Y., Okumura, K. & Ogawa, H. (2004) *J. Invest Dermatol.* **123,** 229–236.
34. Ingber, D. E. (2005) *Proc. Natl. Acad. Sci. USA* **102,** 11571–11572.
35. Helmke, B. P. (2005) *Physiology (Bethesda)* **20,** 43–53.
36. Ingber, D. E. (2003) *Ann. Med.* **35,** 564–577.
37. Balooch, G., Balooch, M., Nalla, R. K., Schilling, S., Filvaroff, E. H., Marshall, G. W., Marshall, S. J., Ritchie, R. O., Derynck, R. & Alliston, T. (2005) *Proc. Natl. Acad. Sci. USA* **102,** 18813–18818.
38. Katsumi, A., Orr, A. W., Tzima, E. & Schwartz, M. A. (2004) *J. Biol. Chem.* **279,** 12001–12004.
39. Swartz, M. A., Tschumperlin, D. J., Kamm, R. D. & Drazen, J. M. (2001) *Proc. Natl. Acad. Sci. USA* **98,** 6180–6185.
40. Milewicz, D. M., Urban, Z. & Boyd, C. (2000) *Matrix Biol.* **19,** 471–480.
41. Timar, J., Diczhazi, C., Ladanyi, A., Raso, E., Hornebeck, W., Robert, L. & Lapis, K. (1995) *Ciba Found. Symp.* **192,** 321–335.
42. Dvorak, H. F. (1986) *N. Engl. J. Med.* **315,** 1650–1659.
43. Haddow, A. (1972) *Adv. Cancer Res.* **16,** 181–234.
44. Grose, R. (2004) *Genome Biol.* **5,** 228.
45. Meyvisch, C. & Mareel, M. (1985) *Invasion Metastasis* **5,** 185–192.
46. Desmouliere, A., Guyot, C. & Gabbiani, G. (2004) *Int. J. Dev. Biol.* **48,** 509–517.
47. Paszek, M. J., Zahir, N., Johnson, K. R., Lakins, J. N., Rozenberg, G. I., Gefen, A., Reinhart-King, C. A., Margulies, S. S., Dembo, M., Boettiger, D., *et al.* (2005) *Cancer Cell* **8,** 241–254.
48. Beil, M., Micoulet, A., von Wichert, G., Paschke, S., Walther, P., Omary, M. B., Van Veldhoven, P. P., Gern, U., Wolff-Hieber, E., Eggermann, J., *et al.* (2003) *Nat. Cell Biol.* **5,** 803–811.